Journal of Applied Electrochemistry (2006) 36:1399–1405
DOI 10.1007/s10800-006-9232-x

Cathodic electrosynthesis of iron oxide films for electrochemical supercapacitors

N. NAGARAJAN and I. ZHITOMIRSKY*
Department of Materials Science and Engineering, McMaster University, 1280 Main Street West, Hamilton, Ontario, Canada L8S 4L7
*(*author for correspondence, fax: + 905-528-9295, e-mail: zhitom@mcmaster.ca)*

Received 27 February 2006; accepted in revised form 18 August 2006

Key words: cathodic electrosynthesis, chitosan, electrochemical supercapacitor, film, iron oxide

Abstract

Cathodic electrosynthesis has been utilized for the fabrication of γ-Fe_2O_3 films, containing chitosan additive as a binder. The films were studied by X-ray diffraction analysis, X-ray photoelectron spectroscopy, scanning electron microscopy, differential thermal analysis, and thermogravimetric analysis. Cyclic voltammetry and chronopotentiometry data showed that the iron oxide films exhibit electrochemical capacitance in the voltage window of −0.9 to −0.1 V vs SCE in 0.25 M Na_2SO_4 and 0.25 M $Na_2S_2O_3$ aqueous solutions. The highest specific capacitance (SC) of 210 F g^{-1} was achieved using 0.25 M $Na_2S_2O_3$ as electrolyte, at a scan rate of 2 mV s^{-1}. The SC decreased with increasing film thickness, scan rate and cycle number. Heat treatment of the films at 140 °C resulted in increasing SC.

1. Introduction

The development of electrochemical supercapacitors (ES) is the subject of intense experimental and theoretical work [1–5]. This research focuses on advanced materials, new fabrication technologies, design and modeling. The performance of ES is strongly dependent on various factors, such as specific capacitance (SC), surface area, particle size and conductivity of the active material, the nature of electrolyte and cell design. Three types of materials have been mostly used for ES: high surface area carbon, metal oxides or hydroxides, and conducting polymers [1, 6–8]. Energy storage mechanisms of ES include double layer capacitance arising from the charge separation at an electrode/electrolyte interface and pseudocapacitance arising from reversible Faradaic reactions or from the surface adsorption of potential determining ions.

Extensive studies have shown that nanostructured metal oxides and hydroxides are promising materials for ES and exhibit high pseudocapacitance. Amorphous hydrous ruthenium oxide ($RuO_2 \cdot nH_2O$) exhibits excellent pseudo-capacitive behavior [8–10]. Although $RuO_2 \cdot nH_2O$ gives high SC, it has a disadvantage of high cost. On the other hand, transition metal oxides, such as NiO [11–13], Co_3O_4 [14], MnO_2 [15–17], Fe_3O_4 [18–21] have been identified as possible electrode materials for electrochemical supercapacitors.

Fe_3O_4 is an attractive candidate for the application in ES. It was shown that SC of Fe_3O_4 depends on the nature of anions and surface area of Fe_3O_4 nanoparticles [18–20]. The highest capacitance of 510 F g^{-1}–Fe_3O_4 in a voltage window of 1.2 V was achieved for the composite Fe_3O_4 – carbon black (3 wt. % Fe_3O_4) electrodes using sodium sulphite as the electrolyte [20]. In contrast, the use of sodium sulphate electrolyte resulted in the SC of 5 F g^{-1}–Fe_3O_4. Brousse and Bélanger [21] prepared Fe_3O_4 powders with high surface area and reported a SC of 75 ± 8 F g^{-1} in 0.1 M K_2SO_4. Thin film Fe_3O_4 electrodes showed a SC of 170 and 25 F g^{-1} in the Na_2SO_3 and Na_2SO_4 electrolytes, respectively [22]. Recently a two-step anodic electrochemical method has been developed for the fabrication of Fe_3O_4 films [23]. The method enabled the formation of the cellular Fe_3O_4 films, providing high electrochemical accessibility and a fast diffusion rate of the electrolyte. The cellular Fe_3O_4 thin films showed rectangular cyclic voltammograms indicative of typical capacitive behavior in the Na_2SO_4 solutions and a SC of 105 F g^{-1}. This study highlighted the importance of the porosity of Fe_3O_4 films, which creates a volume for the diffusion of electrolyte and provides a high surface area for the electrode reactions.

We report herein, the capacitive properties of γ-Fe_2O_3 films prepared by cathodic electrosynthesis and tested in the 0.25 M Na_2SO_4 and 0.25 M $Na_2S_2O_3$ solutions.

2. Experimental procedures

2.1. *Electrodeposition of iron oxide films*

$FeCl_2 \cdot 4H_2O$ and chitosan (Mw = 20 0000, degree of deacetylation 85%) were purchased from Aldrich and used as starting materials. Chitosan was dissolved in a 1% acetic acid solution. Electrodeposition was performed from 5 mM $FeCl_2$ solutions in a mixed ethanol – water (20 vol.% water) solvent, containing 0–0.2 g l^{-1} chitosan. Cathodic deposits were obtained on Pt disks with an area of 1 cm^2 by the galvanostatic method at a current density of 3 mA cm^{-2}. The deposition time was varied in the range of up to 6 min. The electrochemical cell for deposition included a cathodic substrate and a platinum counter-electrode. Deposit weight was studied by weighing the substrates before and after deposition experiments followed by drying at room temperature for 24 h.

2.2. *Deposit composition and microstructure characterization*

The electrolytic deposits were scraped from the electrodes for X-ray diffraction (XRD) study, thermogravimetric analysis (TGA) and differential thermal analysis (DTA). The phase content of the deposits was determined by XRD with a diffractometer (Nicolet I2) using monochromatic Cu K_α radiation at a scanning speed of 0.5 °C min^{-1}. For the XRD studies the deposits were also annealed in air at 140 °C for 1 h. TGA and DTA studies were carried out in air between room temperature and 1000 °C at a heating rate of 5 °C min^{-1} using a thermoanalyzer (Netzsch STA−409). The microstructures of the deposited coatings were studied using a JEOL JSM−7000F scanning electron microscope (SEM). The X-ray photoelectron spectroscopy (XPS) analysis was carried out with a Kratos Axis Ultra spectrometer, using a Al–Kα X-ray source.

2.3. *Electrochemical measurements*

The deposited films were studied using a potentiostat (PARSTAT 2273, Princeton Applied Research) controlled by a computer using a PowerSuite electrochemical software package. Electrochemical characterization of the films was performed using a standard three-electrode cell configuration with either 0.25 M Na_2SO_4 or 0.25 M $Na_2S_2O_3$ aqueous solution as electrolytes. The electrolyte solutions were degassed with purified nitrogen gas before the electrochemical measurements. The surface area of the working electrode was 1 cm^2. The counter electrode was platinum gauze, and the reference electrode was a standard calomel reference electrode (SCE). Cyclic voltammetry (CV) studies were performed within a range of −0.1 to −0.9 V vs SCE at scan rates of 2–100 mV s^{-1}. The SC was calculated using half the integrated area of the CV curve to obtain the charge (Q), and subsequently dividing the charge by the mass of the electrode (m) and the width of the potential window (ΔV):

$$C = Q/m\,\Delta\,V \quad (1)$$

Galvanostatic charge/discharge cycling was performed at constant current densities of 0.4–1 mA cm^{-2}. The obtained chronopotentiograms were used for the calculation of SC from the equation [24]:

$$C = I/(\,\Delta\,V/\,\Delta\,t)m \quad (2)$$

where $\Delta V/\Delta t$ is the average slope of the discharge curve, I is the current.

3. Results

3.1. *Preparation of FeO_x films*

Cathodic deposits were obtained from the 5 mM $FeCl_2$ solutions containing 0–0.2 g l^{-1} chitosan. However, the deposits prepared from pure 5 mM $FeCl_2$ solutions without chitosan exhibited low adhesion. The addition of chitosan to the solutions resulted in improved adhesion and reduced cracking in the as-deposited films. Figure 1 shows the deposit mass as a function of deposition time for the 5 mM $FeCl_2$ solutions, containing 0.2 g l^{-1} chitosan. The results given in Figure 1 indicate that the deposit weight increases with deposition time at a constant current density. The increase in the deposit mass was essentially linear, indicating a constant rate of deposition at a current density of 3 mA cm^{-2}. As deposited and heat-treated at 140 °C films were used for the electrochemical studies.

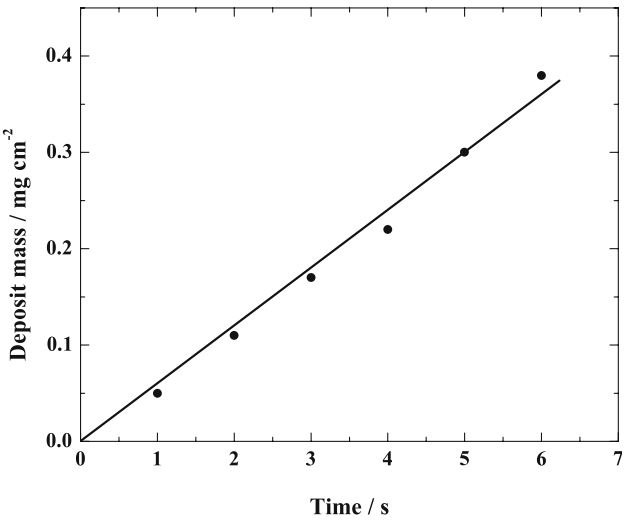

Fig. 1. Deposit mass versus deposition time for the deposits prepared from 5 mM $FeCl_2$ solutions containing 0.2 g l^{-1} chitosan at a constant current density of 3 mA cm^{-2}.

3.1.1. *Deposit composition and microstructure*

As prepared films were studied by XPS in order to ascertain the valence state of iron. The results indicate the formation of Fe^{3+} species. The XPS Fe2p spectrum presented in Figure 2 shows two intense peaks at 711.2 eV and 724.5 eV, assigned to the $Fe2p_{3/2}$ and $Fe2p_{1/2}$ binding energies, respectively. In addition, a satellite peak was found at 719.3 eV. The measured Fe2p binding energies are in a good agreement with the literature values [25–28] for the Fe^{3+} species. It should be noted that the characteristic peak for Fe^{2+} at ~709.3 eV, and the corresponding satellite peak at ~714 eV [26–28] were not observed.

SEM studies revealed the formation of porous films with fine particles, as shown in Figure 3. X-ray studies of as-prepared films (Figure 4) showed peaks of γ-Fe_2O_3 (JCPDS file 39–1346). The peak broadening could be attributed to the small particle size in agreement with the results of the SEM investigations. Similar X-ray diffraction patterns were obtained for the films annealed at 140 °C during 1 h (Figure 4).

Figures 5 and 6 show the TGA and DTA data for the deposits prepared from the 5 mM $FeCl_2$ solutions without and with 0.2 g l^{-1} chitosan. The sample without the polymer (Figure 5) showed a total weight loss of 8.4 wt.% in the temperature range up to 1000 °C with most of the weight loss occurring below ~200 °C. No weight change was observed in the range of 400–1000 °C. The weight loss in this region can be attributed to liberation of the adsorbed water. The corresponding DTA data showed a small endotherm around 100 °C.

TGA studies of the deposits prepared from the 5 mM $FeCl_2$ solutions containing 0.2 g l^{-1} chitosan (Figure 6) showed a total weight loss of ~20.8 wt.%. The TGA data presented in Figure 6 shows two distinct steps in the weight loss in the temperature ranges of 50–200 °C and 200–380 °C. No weight change was observed in the range of 400–1000 °C. The DTA data (Figure 6) shows a broad endotherm at ~100 °C, and an exotherm around 280 °C. It is suggested that the observed endotherm and exotherm correspond to the steps in the weight loss. The results of TGA and DTA studies (Figure 6) indicate co-deposition of iron oxide and chitosan. The total weight loss can be attributed to the dehydration of the deposits and burning out of chitosan. The observed endothermic effect can be attributed to the liberation of the adsorbed water. The exotherm at 280 °C can be related to the burning out of chitosan in agreement with the literature DTA data for the pure polymer [29]. Using the TGA data (Figures 5, 6) the chitosan content in the film, prepared from the 5 mM $FeCl_2$ solutions containing 0.2 g l^{-1} chitosan, was estimated to be ~13.5 wt. %. However, it is important to

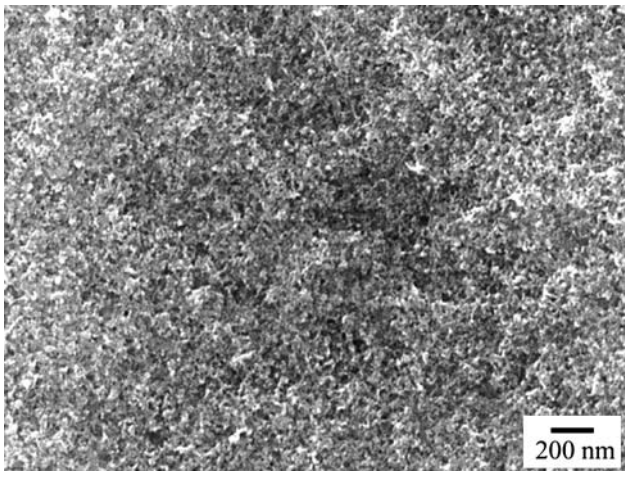

Fig. 3. SEM micrograph showing a film prepared from the 5 mM $FeCl_2$ solution containing 0.2 g l^{-1} chitosan and heat-treated at 140 °C during 1 h.

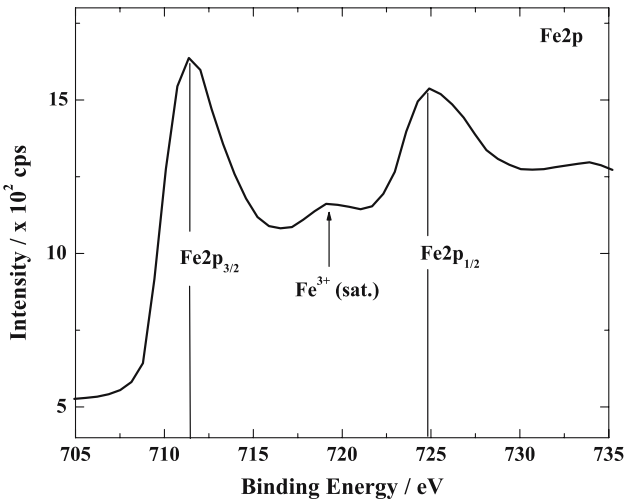

Fig. 2. XPS Fe2p spectra for the film prepared from the 5 mM $FeCl_2$ solution containing 0.2 g l^{-1} chitosan and heat-treated at 140 °C during 1 h.

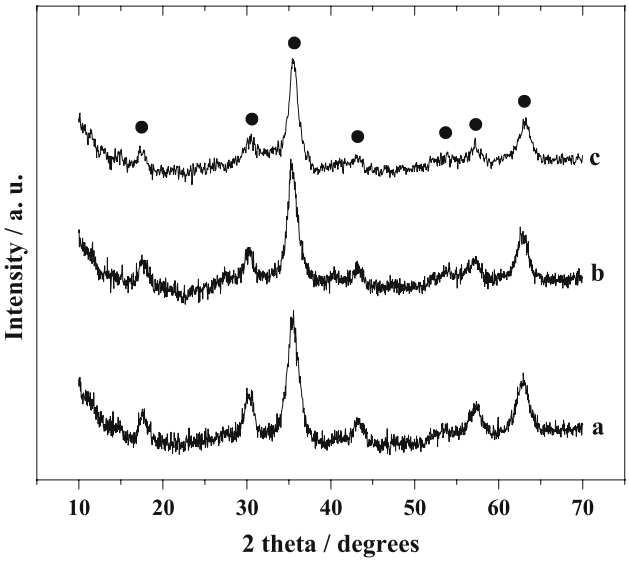

Fig. 4. X-ray diffraction patterns for the films prepared from the 5 mM $FeCl_2$ solutions without chitosan (a) and containing 0.2 g l^{-1} chitosan (b, c): as prepared (a, b) and after heat treatment at 140 h during 1 h (c); • – γ-Fe_2O_3 (JCPDS file 39–1346).

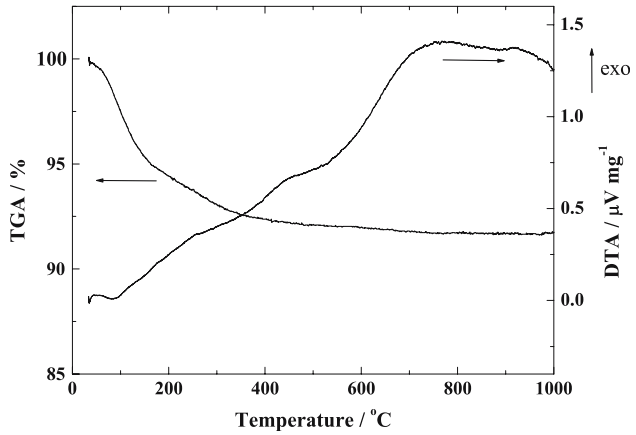

Fig. 5. TGA and DTA data for the deposit prepared from the 5 mM $FeCl_2$ solution without chitosan.

note that the electrosynthesis of inorganic phases can be influenced by polymer [30]. Therefore, more detailed study is necessary in order to find the chitosan content in the films.

3.2. *Electrochemical studies*

The iron oxide films prepared from 5 mM $FeCl_2$ solutions containing 0.2 g l^{-1} chitosan were used for the electrochemical studies. The films were heat treated at 140 °C during 1 h in order to reduce the amount of the adsorbed water and increase the stability of chitosan in aqueous solutions [31]. Cyclic voltammetry has been used to characterize the capacitive behavior of the iron oxide films in the 0.25 M Na_2SO_4 and 0.25 M $Na_2S_2O_3$ solutions. The results of the investigations indicate that a higher SC can be achieved in the 0.25 M $Na_2S_2O_3$ solutions. Figure 7 compares the cyclic voltammograms (CVs) for the 0.1 mg cm^{-2} iron oxide films at a scan rate of 100 mV s^{-1} in the 0.25 M Na_2SO_4 and 0.25 M $Na_2S_2O_3$ aqueous solutions. In both cases, significant SC was achieved within a voltage window of −0.9 to −0.1 V. It is clear from the curves that the SC of the

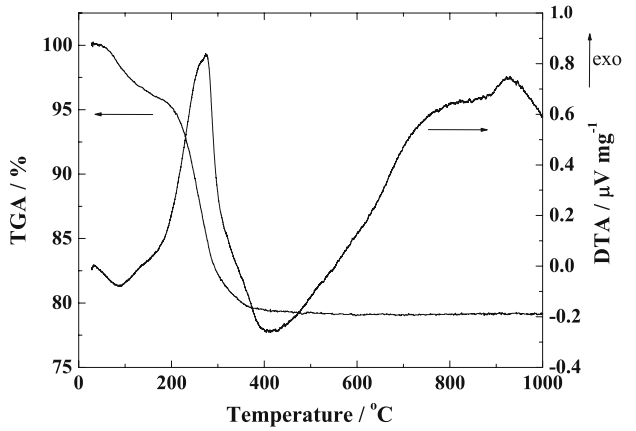

Fig. 6. TGA and DTA data for the deposit prepared from the 5 mM $FeCl_2$ solutions containing 0.2 g l^{-1} chitosan.

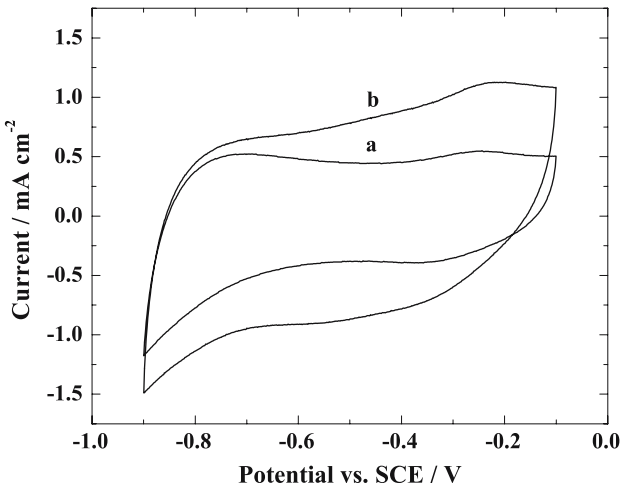

Fig. 7. Cyclic voltammograms for the 0.1 mg cm^{-2} iron oxide films, scanned at 100 mV s^{-1} in 0.25 M sodium sulfate (a) and 0.25 M sodium thiosulfate electrolyte (b). The calculated SC values were found to be 43 and 82 F g^{-1}, respectively.

films is much higher when tested in the 0.25 M $Na_2S_2O_3$ solution, than in the 0.25 M Na_2SO_4 solution. Indeed, the calculated value of SC for the thiosulfate solution is 82 F g^{-1}, almost double the value achieved for the sulfate solution (43 F g^{-1}).

Figure 8 shows the CVs of the 0.2 mg cm^{-2} iron oxide films at varying scan rates in the 0.25 M $Na_2S_2O_3$ solution. The CV curves showed roughly rectangular mirror images, indicating the capacitive behavior. It is also clear from Figure 8 that there are no redox peaks in the range between −0.9 and −0.1 V. The obtained results thus indicate that the iron oxide films prepared by cathodic electrodeposition show the capacitive behavior within the window of −0.9 to −0.1 V in the 0.25 M $Na_2S_2O_3$ solution. The SC values calculated from the CVs were found to be 122, 89 and 70 and 55 F g^{-1} for

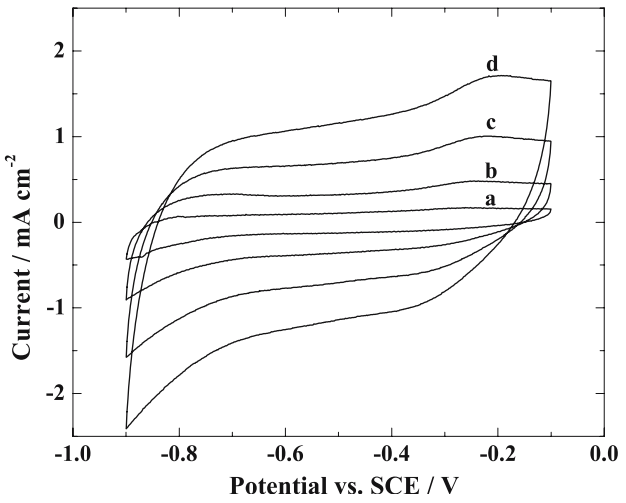

Fig. 8. Cyclic voltammograms for the 0.2 mg cm^{-2} iron oxide films at scan rates of 5 (a), 20 (b), 50 (c) and 100 mV s^{-1} (d). The calculated SC values were found to be 122, 89, 70 and 55 F g^{-1}, respectively.

the scan rates of 5, 20, 50 and 100 mV s^{-1}, respectively. The SC values were also dependent on the film mass. Figure 9 shows the CVs for the iron oxide films of varying mass, scanned at 20 mV s^{-1}. The SC values were found to be 115, 89 and 65 F g^{-1} for 0.1, 0.2 and 0.4 mg cm^{-2} films, respectively.

Figure 10 illustrates the influence of the scan rate, film thickness, and heat treatment on the SC of the iron oxide films. The SC of 210 F g^{-1} was obtained at a scan rate of 2 mV s^{-1} for the iron oxide film with the mass of 0.1 mg cm^{-2} after heat treatment at 140 °C. However, the SC falls rapidly as the scan rate increases in the range of 2–100 mV s^{-1}. The as-prepared films of the same mass showed lower SC, which decreased with the increasing scan rate. Similar behavior was observed for the 0.4 mg cm^{-2} films. The heat-treated sample showed a higher SC at all scan rates, compared to the as-prepared samples. The increase in film mass resulted in the reduced SC (Figure 10).

Figure 11 shows the galvanostatic charge-discharge behavior of heat-treated iron oxide films. The average SC values were found to be 104 and 63 F g^{-1} for the current densities of 0.4 and 1 mA cm^{-2}, respectively. The cycle stability testing was performed at a scan rate of 50 mV s^{-1}. The experimental results presented in Figure 12 indicate the reduction in SC as a result of cycling. The SC derived from the CVs decreased from 95 F g^{-1} for the 2nd cycle to 65 F g^{-1} for the 100th cycle. The cycle stability of the iron oxide films must be improved in the future work.

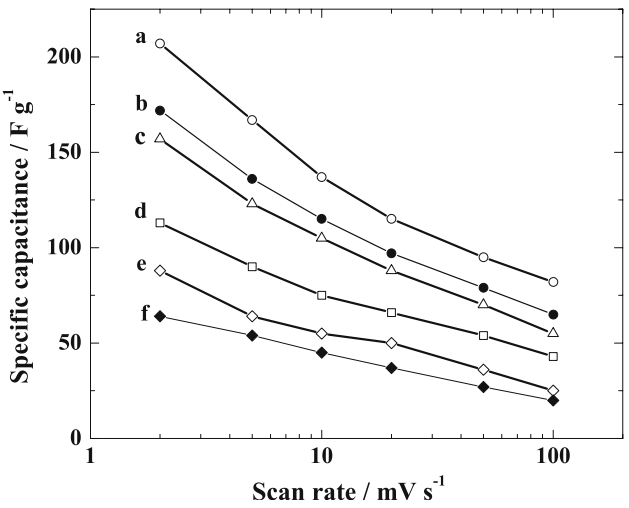

Fig. 10. SC of the iron oxide films as a function of scan rate for deposit mass of 0.1 (a,b), 0.2 (c), 0.3 (d) and 0.4 mg cm^{-2} (e, f): as deposited (b, f) and after heat treatment at 140 °C (a, c, d, e).

4. Discussion

4.1. *Film deposition, composition and microstructure*

In this work the electrosynthesis of iron oxide films was performed from $FeCl_2$ solutions. The linearity of the deposit weight vs time plot (Figure 1) indicates that the deposition process can be controlled so as to form reproducible deposits of a given mass. Furthermore, it is possible to alter the deposit mass by changing the deposition time. The mechanism of cathodic electrosynthesis of oxide/hydroxide materials has been described in the literature [32, 33]. In this method metal ions or complexes are hydrolyzed by electrogenerated base to form colloidal particles in the high pH region at the cathode surface. The particles coagulate to form a cathodic deposit. SEM observations indicate that as-prepared deposits consist of fine particles.

X-ray studies showed crystallinity of the iron oxide deposits. The X-ray diffraction pattern was attributed to γ-Fe_2O_3. Note that it is difficult to distinguish between the X-ray diffraction patterns of nanostructured

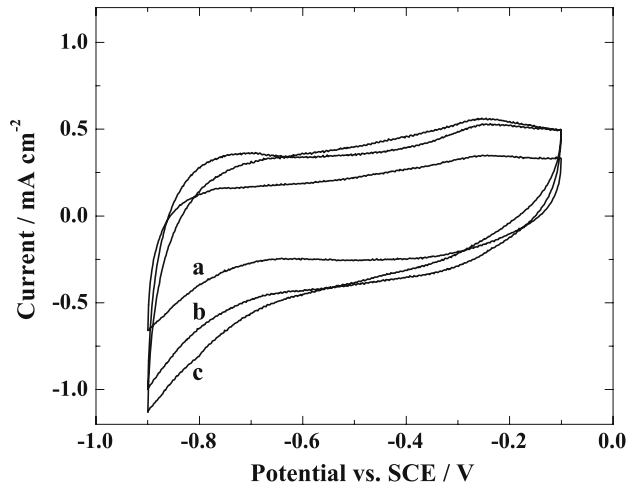

Fig. 9. Cyclic voltammograms for the iron oxide films at a scan rate of 20 mV s^{-1} and deposit mass 0.1 (a), 0.2 (b) and 0.4 mg cm^{-2} (c). The calculated SC values were found to be 115, 89 and 65 F g^{-1}, respectively.

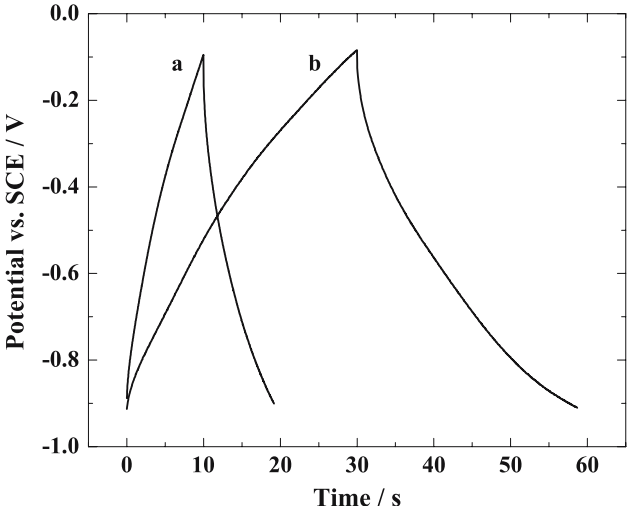

Fig. 11. Charge-discharge curves for the 0.2 mg cm^{-2} iron oxide films obtained at a constant current density of 1.0 (a) and 0.4 mA cm^{-2} (b). The calculated SC values were found to be 63 and 104 F g^{-1}, respectively.

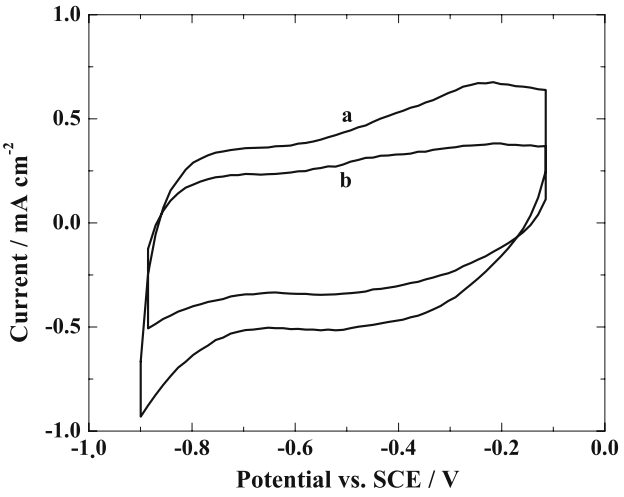

Fig. 12. Cyclic voltammograms for the 0.1 mA cm^{-2} iron oxide film at a scan rate of 50 mV s^{-1} for the 2nd (a) and 100th (b) cycles. The calculated SC values were found to be 95 and 65 F g^{-1}, respectively.

γ-Fe_2O_3 and Fe_3O_4 due to the peak broadening. Moreover, γ-Fe_2O_3 and Fe_3O_4 form solid solutions. However, XPS data indicate the formation of Fe^{3+} species only. The XPS results were supported by the TGA results. Indeed, no weight gain was observed related to the $Fe_3O_4 \rightarrow Fe_2O_3$ transformation [34] during heating in air. It is suggested that Fe^{2+} species are oxidized in solutions or during deposit drying in air to form γ-Fe_2O_3. The possibility of the room temperature formation of γ-Fe_2O_3 was also reported in the previous investigation [35]. However, in the previous investigation, γ-Fe_2O_3 films were prepared from the $FeCl_3$ solutions [35]. We reported the superparamagnetic properties of the γ-Fe_2O_3 and composite films [35].

The active electrode materials for ES usually include binders and conductive additives [16]. In this work chitosan was used as a binder in order to improve the film adhesion to the substrates. The results of TGA and DTA analysis (Figures 5 and 6) indicate co-deposition of chitosan and iron oxide. The mechanism of chitosan electrodeposition has been previously studied [36]. Chitosan is soluble in water only when protonated in acidic solutions. At low pH, chitosan becomes a cationic polyelectrolyte [36, 37]

$$\mathrm{Chit-NH_2 + H_3O^+ \rightarrow Chit-NH_3^+ + H_2O} \qquad (3)$$

Under the action of an electric field, the charged chitosan macromolecules move towards the cathode surface. At the cathode, the reduction of water causes the local pH increase according to the reaction:

$$\mathrm{2H_2O + 2e^- \rightarrow H_2 + 2OH^-} \qquad (4)$$

It is suggested that the chitosan loses its charge and forms an insoluble deposit on the cathode surface:

$$\mathrm{Chit-NH_3^+ + OH^- \rightarrow Chit-NH_2 + H_2O} \qquad (5)$$

It is known that heat treatment of chitosan films at temperatures exceeding 90 °C can result in the improved water resistance due to the formation of crosslinks and crystallites in the films [31]. In this work, the iron oxide films containing chitosan as a binder were heat treated at 140 °C in order to improve the water resistance of chitosan. Iron oxide films of various thicknesses were used for the electrochemical studies.

4.2. *Capacitive behavior of the iron oxide films*

The iron oxide films prepared by the cathodic electrodeposition method exhibited SC as high as 210 F g^{-1}, which exceeds the SC values for the pure iron oxide films reported in the literature. The results indicate that iron oxide is a promising material for application in ES. However, the high SC capacitance was observed in films of relatively low mass. The SC decreased with increasing film thickness, increasing scan rate or galvanostatic charge-discharge rate. Similar drop in SC has been observed in other investigations and is generally attributed to either the resistance due to ionic depletion in the electrolyte [8, 10] or due to the intrinsic resistance of the electrode [16].

Moreover, cycling resulted in significant decrease in SC. The important task is to increase the total capacitance by the increase in the amount of the active material and prevent the reduction in SC with increasing film thickness. It is suggested that SC of iron oxide can be utilized better in porous composite materials, containing iron oxide nanoparticles and conducting additives. Therefore, further work must be focused on co-deposition of iron oxide with conductive additives and increase in porosity of the composite films.

We suggest that the mechanism that provides SC of γ-Fe_2O_3 is similar to that proposed for Fe_3O_4 [22]. It was suggested that iron oxide provides favorable specific sites for the adsorption of anions and acts as a catalyst for the redox reactions. The possible reaction that leads to the pseudo-capacitive behavior of iron oxide films in thiosulfate solutions is [22]:

$$\mathrm{S_2O_3^{2-} + 3H_2O + 4e^- \leftrightarrow 2S + 6OH^-} \qquad (6)$$

A more detailed study is required in order to clarify the influence of the iron oxide film on the thiosulfate redox reactions.

5. Conclusions

Cathodic electrodeposition method has been developed for the fabrication of iron oxide films, containing chitosan additive as a binder. The amount of the deposited material can be controlled by the variation of the deposition time. The results of XRD, XPS, SEM, TGA and DTA indicate the formation of γ-Fe_2O_3 films. The iron oxide films exhibited the capacitive behavior within the window of −0.9 to −0.1 V vs SCE in the 0.25 M Na_2SO_4 and 0.25 M $Na_2S_2O_3$ aqueous solutions. However, higher SC was observed using the 0.25 M

$Na_2S_2O_3$ as an electrolyte. The highest SC of 210 F g^{-1} was achieved for 0.1 mg cm^{-2} films at a scan rate of 2 mV s^{-1}. Heat treatment of the films at 140 °C resulted in increasing SC. The SC decreased with increasing film thickness, scan rate and cycle number.

Acknowledgement

The authors gratefully acknowledge the financial support of the Natural Science and Engineering Council of Canada.

References

1. B.E. Conway, *Electrochemical Supercapacitors, Scientific Fundamentals and Applications* (Kluwer Academic Publishers, Netherlands, 1999).
2. R.A. Higgins, *Solid State Ionics* **134** (2000) 179.
3. R. Kötz and M. Carlen, *Electrochim. Acta* **45** (2000) 2483.
4. B. Fang, Y-Z. Wei, K. Maruyama and M. Kumagai, *J. Appl. Electrochem.* **35** (2005) 229.
5. H. Talbi, P-E. Just and L.H. Dao, *J. Appl. Electrochem.* **33** (2003) 465.
6. F. Beck and M. Dolata, *J. Appl. Electrochem.* **31** (2001) 517.
7. S. Sarangapani, B.V. Tilak and C.P. Chen, *J. Electrochem. Soc.* **143** (1996) 3791.
8. J.P. Zheng, P.J. Cygan and T.R. Jow, *J. Electrochem. Soc.* **142** (1995) 2699.
9. J.P. Zheng and T.R. Jow, *J. Electrochem. Soc.* **142** (1995) L6.
10. H. Kim Il., J-H. Kim and K-B. Kim, *Electrochem. Solid State Lett.* **8** (2005) A369.
11. V. Srinivasan and J.W. Weidner, *J. Electrochem. Soc.* **144** (1997) L210.
12. K-C. Liu and M.A. Anderson, *J. Electrochem. Soc.* **143** (1996) 124.
13. K-W. Nam and K-B. Kim, *J. Electrochem. Soc.* **149** (2002) A346.
14. V. Srinivasan and J.W. Weidner, *J. Power Sources* **108** (2002) 15.
15. S-F. Chin, S-C. Pang and M.A. Anderson, *J. Electrochem. Soc.* **149** (2002) A379.
16. M. Toupin, T. Brousse and D. Belanger, *Chem. Mater.* **14** (2002) 3946.
17. B. Djurfors, J.N. Broughton, M.J. Brett and D.G. Ivey, *Acta Mater.* **53** (2005) 957.
18. L-R. Shiue, N-L. Wu, D-S. Wu, C-W. Chao, Y-P. Lan, United States Patent No: US 6,678,147 B2, Jan. (2004).
19. S-Y. Wang and N-L. Wu, *J. Appl. Electrochem.* **33** (2003) 345.
20. N-L. Wu, S-Y. Wang, C-Y. Han, D-S. Wu and L-R. Shiue, *J. Power Sources* **113** (2003) 173.
21. T. Brousse and D. Bélanger, *Electrochem. Solid State Lett.* **6** (2003) A244.
22. S-Y. Wang, K-C. Ho, S-L. Kuo and N-L. Wu, *J. Electrochem. Soc.* **153** (2006) A75.
23. K.W. Chung, K-W. Kim, S-H. Han and H. Lee, *Electrochem. Solid State Lett.* **8**(n5) (2005) A259.
24. Y-T. Wu and C-C. Hu, *J. Electrochem. Soc.* **151** (2004) A2060.
25. J. Hu, G. Chen and I.M.C. Lo, *Water Research* **39** (2005) 4528.
26. P.C.J. Gratt and M.A.J. Somers, *App. Surf. Sci.* **100–101** (1996) 36.
27. Y. Gao, Y.J. Kim, S.A. Chambers and G. Bai, *J. Vac. Sci. Technol. A* **15** (1997) 332.
28. A.P. Grosvenor, B.A. Kobe, M.C. Biesinger and N.S. McIntyre, *Surf. Interface Anal.* **36** (2004) 1564.
29. J. Nunthanid, S. Puttipipatkhachorn, K. Yamamoto and G.E. Peck, *Drug Develop. Ind. Pharm.* **27** (2001) 143.
30. X. Pang, I. Zhitomirsky and M. Niewczas, *Surf. Coatings Tech.* **195** (2005) 138.
31. L.Y. Lim and L.S.C. Wan, *Drug Develop. Ind. Pharm.* **21** (1995) 839.
32. G.H.A. Therese and P.V. Kamath, *Chem. Mater.* **12** (2000) 1195.
33. I. Zhitomirsky, *Adv. Coll. Interf. Sci.* **97** (2002) 279.
34. R.M. Cornell and U. Schwertmann, *The Iron Oxides* (Wiley-VCH Verlag GmbH and Co, Weinheim, 2003), pp. 402.
35. J. Cao, I. Zhitomirsky and M. Niewczas, *Mater. Chem. Phys.* **96** (2006) 289.
36. L-Q. Wu, A.P. Gadre, H. Yi, M.J. Kastantin, G.W. Rubloff, W.E. Bentley, G.F. Payne and R. Ghodssi, *Langmuir* **18** (2002) 8620.
37. X. Pang and I. Zhitomirsky, *Mater. Chem. Phys.* **94** (2005) 245.